IEEE Transactions on Robotics (T-RO) paper, presented at ICRA 2026, Vienna, Austria. Cite as T-RO paper.

3D-Printable Crease-Free Origami Vacuum Bending Actuators for Soft Robots

Zhanwei Wang, *Student Member, IEEE*, Huaijin Chen, Syeda Shadab Zehra Zaidi, Ellen Roels, Hendrik Cools, Bram Vanderborght, *Senior Member, IEEE*, and Seppe Terryn, *Member, IEEE*

***Abstract*—While vacuum-based bending actuation offers benefits such as safety and compactness in soft robotics, it is often overlooked due to its limited actuation pressure, which restricts both bending angle and force output. This study presents a crease-free, origami-inspired vacuum bending actuator that advances both state-of-the-art vacuum bending actuators and traditional origami deformation principles by introducing orderly self folding through optimized stiffness distribution. Achieved through finite element method, this design provides several advantages: 1) Self-folding allows for high bending angles (up to 138°) in a compact form. 2) The crease-free design facilitates 3-D printing from a single soft material using a consumer-level fused filament fabrication printer, specifically thermoplastic polyurethane with a Shore hardness of 60 A, potentially higher flexibility and durability. 3) The compact configuration enables modular design, supporting reconfiguration as demonstrated in adaptable locomotion soft robots. 4) The large bending angles allow the actuator to wrap around objects, offering extensive contact compared to other designs. This capability, combined with its vacuum-driven mechanism, enables synergy with self-closing suction cups in an octopus-like vacuum gripper, providing large versatility and grasping force for handling a wide range of objects, from small, irregular shapes to larger, flat items.**

***Index Terms*—3-D printing, experimentally validated, origami, pneumatic actuator, soft robot, vacuum bending.**

I. Introduction

BENDING actuators are vital components in soft robotics. They enable grasping motions in soft grippers, facilitate the creation of soft manipulators, and function as legs in locomotion for soft robots [1], [2], [3]. Apart from actuation via smart materials, such as electrical [4], [5], [6], magnetic [7], [8], [9], thermal [10], [11], [12], or photo-responsive materials [13], [14], [15], the most affordable and broadly used bending actuators are driven by fluidic pressure or tendon. Fluidic bending actuators typically consist of internal deformable hollow chambers that dictate the desired output motions. In contrast, tendon-driven bending actuators use tension cables to mimic the function of muscles or tendons. Compared to tendon-driven actuators, fluidic bending actuators generate a more uniform force along the entire actuator. In addition, unlike tendon-driven systems, pneumatic actuators generate force in multiple directions. This multidirectional and distributed force generation makes pneumatic actuators highly versatile and extensively utilized in soft robotics.

Among fluidic actuators, positive pressure pneumatic systems are often used since unlimited positive pressure can generate higher force and faster actuation [16]. Vacuum-driven actuators are limited in the force and speed they can generate, primarily due to the constrained negative pressure they can achieve (e.g., typically up to 1 bar below atmospheric pressure). Furthermore, their deformations are less predictable due to buckling. Nevertheless, compared to pneumatic actuators, vacuum actuators are inherently fail-safe. This is because compressed air, if leaked, can dislodge debris or particles that may pose a risk to delicate human tissues such as the eyes. Furthermore, vacuum actuators are highly compatible with suction cups, which are increasingly popular due to their compactness and strong adhesive forces, a capability that can compensate for the limited force transmission of vacuum actuators [17], [18], [19], [20]. Likewise, other vacuum-related functionalities can be seamlessly integrated, such as vacuum jamming for achieving variable stiffness in soft robots [21], [22]. In contrast to positive pressure actuators, vacuum actuators decrease in volume during actuation instead of expanding. Consequently, their compactness enhances their integration and allows them to be used in confined spaces.

Because of the restricted negative pressure, vacuum bending actuators demonstrate considerable limitations in bending angles [2], [23], [24], [25], constraining the performance in practical grasping or moving tasks. Thus, many vacuum grippers, originated from mimicking octopus tentacles, often use tendon or pressurization to drive bending motions, although the primary grasping force contribution arises from the mounted vacuum suction cups [2], [26], [27]. This results in more intricate robotic systems. This underscores the demand for advanced vacuum actuators capable of achieving greater bending angles, which

Received 13 January 2025; revised 2 June 2025; accepted 22 June 2025. Date of publication 15 July 2025; date of current version 1 August 2025. This work was supported by the EU Project SHINTO under Grant 101057960 and in part by the Belgium Builds Back Circular project SNAP under Grant FOD171. The work of Zhanwei Wang and Huaijin Chen was supported by China Scholarship Council (CSC). The work of Syeda Shadab Zaidi was supported by ITN project SMART under Grant 860108. This article was recommended for publication by Associate Editor N. Correll and Editor H. Zhao upon evaluation of the reviewers' comments. *(Corresponding author: Zhanwei Wang.)*

Zhanwei Wang, Huaijin Chen, Ellen Roels, Hendrik Cools, and Bram Vanderborght are with the Brubotics, Vrije Universiteit Brussel and IMEC, 1050 Elsene, Belgium (e-mail: zhanwei.wang@imec.be).

Syeda Shadab Zehra Zaidi is with the Biorobotics Institute, Scuola Superiore Sant'Anna (SSSA), 56127 Pisa, Italy.

Seppe Terryn is with the Brubotics, Vrije Universiteit Brussel and IMEC, 1050 Elsene, Belgium, and also with the Physical Chemistry and Polymer Science, Vrije Universiteit Brussel, 1050 Elsene, Belgium.

This article has supplementary downloadable material available at https://doi.org/10.1109/TRO.2025.3588726, provided by the authors. A video can also be accessed via https://www.youtube.com/watch?v=ZAHmhGE_f.M

Digital Object Identifier 10.1109/TRO.2025.3588726

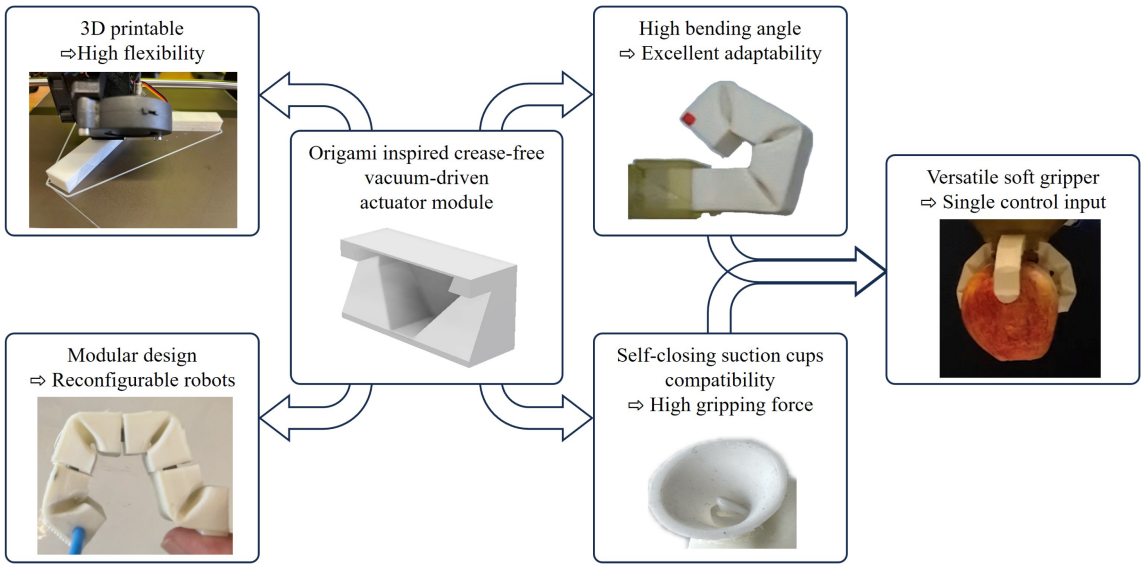

Fig. 1. Overview of the BSVA. Advantages of the design include: 1) The crease-free design allows high-quality 3D printing fabrication and versatile designs. 2) Modular structure allows for configurable robots. 3) Self-folding based on origami principle enables high bending angle. 4) Vacuum actuation ensures seamless integration with self-closing suction cups. 5) Integrated with self-closing suction cups, results in octopus-tentacle-like versatile grippers that adaptively manipulate various objects with a single vacuum control system.

would lead to simplified vacuum-only systems that combine vacuum actuators with vacuum suction cups and/or vacuum-based stiffness modulation.

Incorporating (un)folding techniques inspired by origami or kirigami into bending actuators opens new avenues for enhancing bending performance and integrating intelligent functions into vacuum actuators. Origami, seen in animals and plants, not only enables significant folding and bending, but also incorporates functions such as bistable mechanisms similar to those observed in earwig wings. This inspires a surge of structural intelligence in academia [28], [29], [30]. More specifically in soft robots, examples of functions enabled by origami include in situ stiffness manipulation for tuning force or sensitivity [31], a linear artificial muscle capable of high strain and stress [32], a reconfigurable suction gripper that can undergo flexible shape changes [33], and innovative applications like energy-efficient bistable sensor placement on branches [34]. Zhang et al. [35] proposed the development of soft origami robots using programmable and processable multifunctional elastomeric sheets, laying a sturdy foundation for the rapid advancement of intelligent robots.

In contrast to traditional pressurized pneumatic actuators, origami actuators exhibit minimal strains and hysteresis, primarily relying on folding and unfolding rather than stretching, which enhances their dynamic performance. However, conventional origami machines usually require stiff materials (e.g. plastics, metals, and papers) with premade creases to achieve controlled folding trajectories [36]. While this origami method enables the creation of continuum-deforming structures akin to fingers [37] or trunk-inspired designs [38] in rigid robotics, its applicability within soft robots is limited, as they depend on soft elastomer materials for their adaptability and safety. Nevertheless, several origami soft robots have been researched [39], [40], [40], [41], [42]. However, the design flexibility and scalability of these origami-based soft robots are constrained by the use of linkages or premade creases in their design, which leads to complex manufacturing processes often necessitating multimaterial approaches and labor-intensive manual work. Molding with varied thickness in elastomers can produce airtight pneumatic actuators, such as soft twisting actuators [43]. However, their actuation is usually limited to linear shrinkage or expansion and tends to generate low force, while offering significant flexibility.

This study presents a novel design for an origami-inspired vacuum bending actuator that is free of creases (see Fig. 1). Although it was based on the origami deformation principle, a significant progress is that no crease was required to be premade in the structure due to proper stiffness distribution. The actuator itself forms temporary creases during actuation. This innovative crease-free design has multiple advantages. 1) Due to its orderly self folding behavior, this compact actuator achieves higher bending angles than other vacuum-based actuators, as demonstrated through extensive characterization, with bending performance comparable to that of a human finger. 2) Its compact configuration enables the application of a modular design to the origami-inspired vacuum bending actuator, opening up possibilities for reconfiguration. This modular and reconfiguration approach is assisted by vacuum, which generates cohesive forces between the modules. These capabilities are demonstrated on a reconfigurable locomotion robot. 3) The crease-free design potentially improves surface contact flexibility by eliminating fixed folding tracks and enhances durability by reducing the risk of crack propagation along premade creases. In addition, it enables airtight fabrication of the actuator via fused filament fabrication (FFF) 3-D printing using a single soft elastic material. This is demonstrated through fabrication with thermoplastic

polyurethane (TPU), which possesses a Shore hardness of 60 A, considerably softer than the filaments commonly used in soft robotics, most of which exhibit Shore A hardness values exceeding 80. Consequently, 3-D printing with this TPU posed challenges, necessitating custom modifications and configurations of the 3-D printer, as detailed in the article. The flexibility of the TPU enhances the adaptability of the actuator, reduces its tendency to buckle, and enables smooth pressure-driven bending motion with reliable control. 4) Finally, the compatibility and synergy of this new vacuum-driven actuator with suction cups, in particular a new type of self closing suction cups, is demonstrated in an octopus-like tentacle vacuum gripper capable of grasping irregular and flat objects.

II. Materials and Methods

This study aimed to develop a 3-D-printed, origami-inspired, bending soft vacuum-driven actuator (BSVA). As detailed later in this paper, these BSVAs can be employed in various soft robots, including grippers, locomotion robots, and configurable modules. Initially, the materials, design, and fabrication of the BSVA are presented. FFF was utilized to manufacture the BSVA in a single print using a single TPU material, specifically Recreus Filaflex 60 A. Due to the high flexibility of this material, printing smooth and airtight structures with FFF poses challenges. Therefore, the necessary printer modifications and 3-D printing parameters are discussed in detail.

A. Material Selection and Characterization

Recreus Filaflex 60 A is softer than other common TPU filaments, such as NinjaFlex, which has a Shore hardness of 85 A. Recreus, Inc. supplies this soft TPU filament (1.75 mm diameter). In this article, this soft elastomer is selected because it enhances adaptability and reduces the required actuation power, which is crucial for vacuum actuation since the maximum pressure difference between the actuator and the environment is limited to 1 atm. Although the mechanical properties are provided in the material documentation of Recreus, standard compression (ASTM D575) and tension (ASTM D412) tests were conducted to investigate the mechanical properties of printed TPU samples. ASTM D575 method is used to characterize rubber properties in compression, while ASTM D412 is used to evaluate the tensile properties of vulcanized thermoset rubbers and thermoplastic elastomers. The tension and compression samples were 3-D printed using a solid infill with a concentric printing pattern. As demonstrated in Fig. 2, the printed TPU material samples have an obvious nonlinear behavior during the strain range approximately from 30% to 110%, while a relatively linear stress–strain relation in both the small strain and large strain range. This hyperelastic material property can be characterized by a polynomial model with parameters: $C_{10} = 1.31938144$, $C_{01} = 0.08074091889$, $C_{20} = -0.01073863042$, $C_{11} = 0.120896547$, $C_{02} = -0.544133955$. Based on the experimental results, Young's modulus of 6.65 MPa can be derived via linear regression in the 0% to 25% strain window.

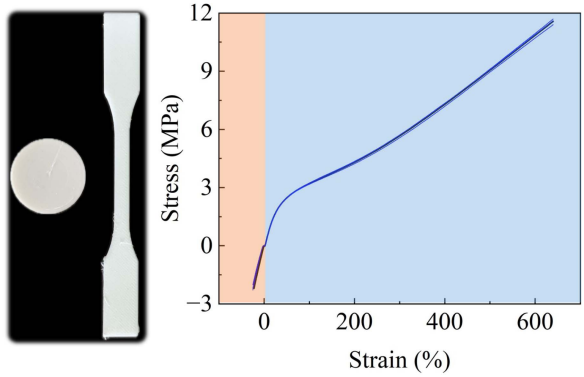

Fig. 2. Quasi-static material mechanical property tests are conducted on printed TPU specimens according to compression test ASTM D575 (orange color range) and tensile test ASTM D412 (blue color range). The circular samples were used for compression testing, while the dogbone-shaped samples were prepared for tensile testing.

B. Design of the Crease-Free Vacuum Bending Actuator

The design of the crease-free vacuum bending actuator considers key aspects such as durability, fabrication, flexibility, and actuation. Conventional origami machines typically rely on premade creases created by folding or variations in shell thickness. The folding method can lead to shell fragility due to crack propagation, increase the likelihood of leaks, and impose limits on the minimum thickness. Repeated folding at the creases reduces durability. The thickness variation method requires relatively thicker shells to create the desired thickness differences, which can compromise overall flexibility. Since soft robots are typically made from elastomers, where flexibility and conformability are essential for effective interaction with objects and environments, the presence of creases restricts deformation and elasticity, thus limiting flexibility.

While many soft robots can be efficiently molded or 3-D printed, the inclusion of creases hinders the feasibility of automated fabrication methods like 3-D printing. Creases reduce the thickness of actuator walls, compromising airtightness, and complicate nozzle trajectories, leading to increased extrusion and retraction frequency and ultimately poor print quality.

Furthermore, vacuum bending actuator behavior involves structural shrinkage and material compression. When the origami structure is formed with premade creases, the elastic restoring force is limited. Without sufficient elasticity, the actuator cannot reliably recover its initial shape upon vacuum release, necessitating the use of an overpressure source that complicates the system. To address these challenges, a crease-free design approach is proposed.

In traditional origami designs, such as the folding box shown in Fig. 3(a), creases are manually created to locally reduce the default stiffness of a sheet. When subjected to a compressive force parallel to the sheet's surface, creased sheets fold more easily and compactly, whereas smooth sheets only exhibit relative bending. By incorporating properly distributed creases, a sheet can be engineered to exhibit multiple directional stiffnesses. Under compression or surface pressure, such a sheet folds

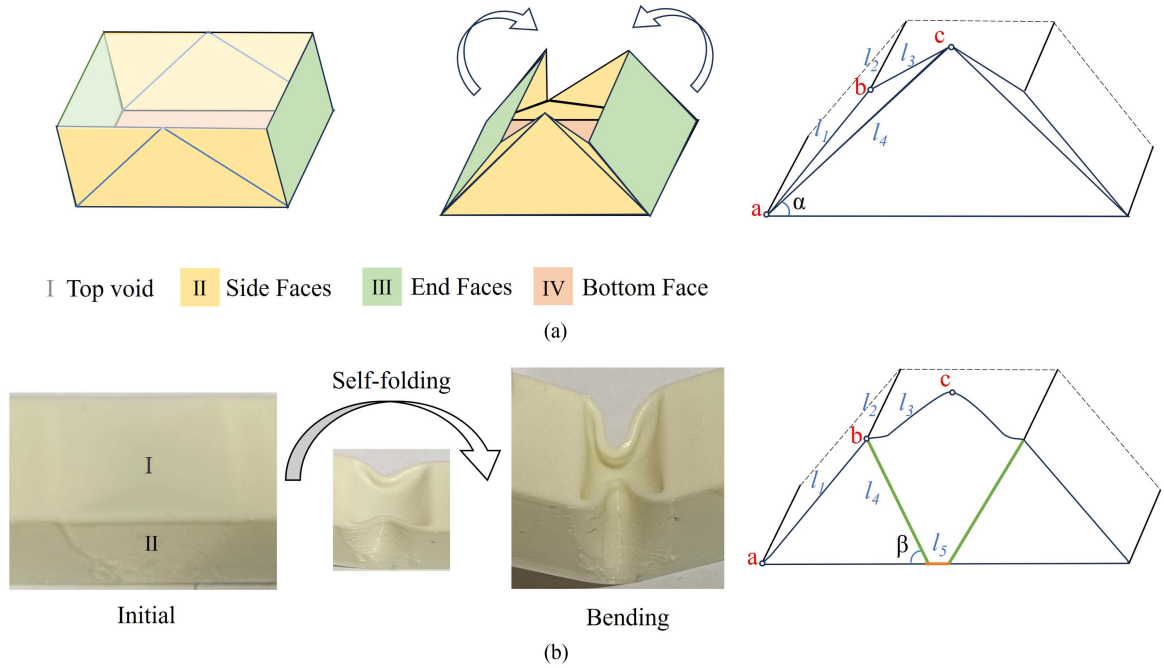

Fig. 3. Origami-based crease-free vacuum bending structure. (a) Schematic diagram of an origami box. The top face (transparent) is considered a void surface, yellow faces with pre-made creases are side faces, and green sheets are end faces. (b) A section of the 3-D-printed bending actuator, the top face (transparent) and side faces (yellow) self fold under air pressure and generate bending behavior.

sequentially along the premade creases. Thus, the creases can be assumed needed to enable directional stiffness by reducing default stiffness.

Since the key mechanism lies in achieving a proper stiffness distribution, and creases are unsuitable for elastomers, pneumatic actuation, and 3-D printing, alternative methods are required. Instead of reducing stiffness, enhancing partial or directional stiffness can be employed to create a similar stiffness distribution. Meanwhile, because of the lower default stiffness of elastomers, moderate stiffness enhancement will not affect compliance and flexibility. Different strategies can achieve this, including varying material thickness, multimaterial compositions, or integrating stimulus–responsive materials. In this study, a structural design approach is selected to generate the required stiffness distribution, and fundamentally verify the effectiveness of the proposed approach.

The conceptual design of the bending module is inspired by the folding behavior of an origami box. Specifically, the design mimics the fundamental stiffness distribution of an origami box. Fig. 3(a) depicts the schematic diagram of an origami box. The origami box, e.g., the rectangular cuboid, consists of four vertical faces, with two of them having crossed creases. The stiffness of the top face (transparent) I is lowest since it is void, the stiffness of face II is lower than III due to a pair of crossed creases. When a horizontal force compresses the box, face II is more susceptible to stress and folds. Subsequently, faces III tilt towards each other and gradually incline closer to the bottom. If multiple origami boxes are attached via face III, they can generate a bending motion. Maximum folding with minimal force is achieved when the creases are as long as possible. However, point c [see Fig. 3(a)] cannot cross the symmetrical middle line because this would cause interference between the two side faces (yellow) during folding. Consequently, the relationships between the dimensions of the origami box can be described as follows:

$$l_4^2 = l_1^2 + l_3^2 \tag{1}$$

$$\alpha = \tan^{-1}(l_1/l_3) \tag{2}$$

$$l_2 \geq l_3. \tag{3}$$

The top face (transparent) is designed to be as thin as possible to emulate the void top opening of an origami box. The side faces (yellow) exhibit higher stiffness than the top face due to their increased thickness and smaller surface area. The width of the bottom of the side face (l_5) should be smaller than l_3 to prevent it from yielding under air pressure. However, the thickness must not be too high to avoid hindering the elastic bending of l_5. As a result, the crease shown in Fig. 3(a) is absent here; instead, l_4 marks the boundary of the slopes of the end faces (green) to differentiate stiffness between l_3 and l_5. The dimensional relationships of the vacuum bending module can be described as follows:

$$l_3 = l_4 \cdot \cos(\beta) + 0.5 \cdot l_5 \tag{4}$$

$$l_2 \geq l_3. \tag{5}$$

The end faces (green) is designed thicker to connect with adjacent module sections, forming a larger vacuum-bending actuator. This increased thickness enhances their stiffness to support fluidic channels, creating a connection to the vacuum source. Following this design in Fig. 3(a), the bending module deforms like the origami box, which is confirmed through finite element method (FEM) modeling in the next section. As will be

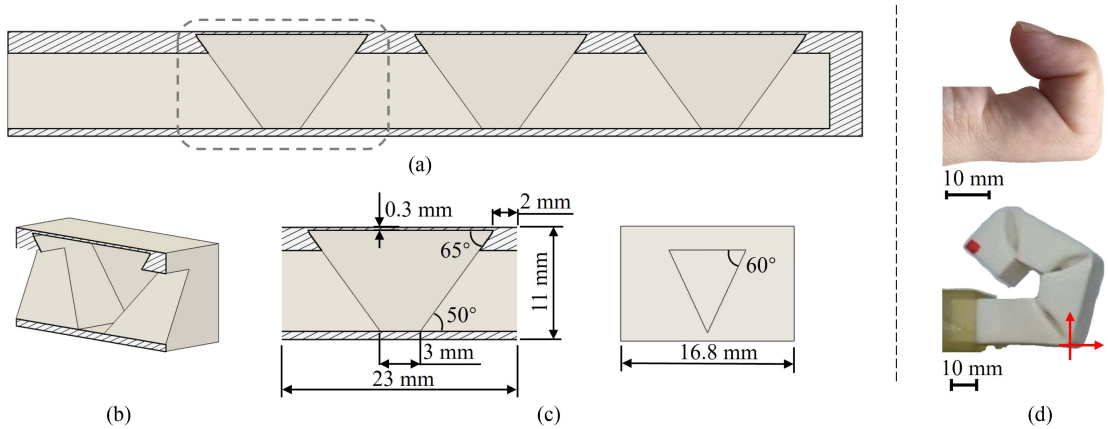

Fig. 4. BSVA. (a) Section view of BSVA geometrical model. (b) Section view of a segment of BSVA. (c) The dimensions of a segment of the BSVA. (d) BSVA is compared to a bending human finger.

discussed in Section D, the minimal wall thickness of horizontal and vertical planes, is 0.3 and 0.4 mm, respectively. Taking these design restrictions, the dimensions of the vacuum bending module as depicted in Fig. 4 are selected.

C. Structural Mechanics Analysis

FEM modeling was performed on ANSYS to evaluate the design of the vacuum bending module deformation since the influence of top surface and thickness were unknown, which is different from a regular origami box. The ratio between the longest edge and the shortest edge is less than 70, which may not cause a singularity issue. Therefore, the model is analyzed using structural mechanics. The geometric model of a BSVA module was built and imported from Solidworks and did fillet to sharp corners. To reduce computation cost, the geometric model is cut in half since it is symmetric, and an elastic material model is used with Young's modulus of 6.65 MPa, and Poisson's ratio of 0.39. Frictional contacts were defined for mating faces, with the model fixed on one side and pressure applied to all other faces. The mesh contained 70 042 elements. A uniform mesh size of 0.4 mm was used for the entire body and a refined 0.2 mm mesh size for the top and back faces using face sizing. The analysis was carried out in Static Structural mode with 150 substeps.

D. 3-D Printer Modification and Configuration

Whereas the design of the vacuum bending module allows both formative and additive manufacturing, the latter is selected. Formative manufacturing, e.g., molding, is extensively used to manufacture fluid soft robots. However, multistage molding is predominantly employed for creating hollow structures, which are crucial for pneumatically driven soft robots. This is exemplified in the fabrication of a manually fabricated vacuum artificial muscle [32] and a flipping robot [1]. This multistage approach creates weak interfaces between parts that were molded in different stages. As a result, the soft robots produced using this method have a limited lifespan due to delamination at these interfaces. Conversely, recent advancements in additive manufacturing on the material and system level have spurred research on 3D-printed soft robots [44], [45], [46], [47], [48], [49], [50], [51]. Nevertheless, the print materials used in these examples have limited flexibility (>Shore A 70). While stereolithography (SLA) offers high-resolution fabrication, the available soft resins are often limited in flexibility and elasticity. Some silicone-like or silicone-based resins provide high stretchability, but they tend to be either too viscous for fabricating thin-shell structures, insufficiently elastic, or prohibitively expensive for practical robotic applications [52]. Moreover, for pneumatic robots with complex internal cavities, the need for support and the difficulty of their removal pose additional challenges, increasing the risk of compromised airtightness. On the other hand, FFF faces challenges due to the compressibility of flexible filaments, leading to issues such as 1) filament extrusion failure due to too little pressure build-up or buckling; 2) flow rate fluctuation due to uncontrolled feeding; 3) nozzle clogging and 4) oozing due to slow retraction; 5) overhang printing failure, stringing or other quality issues during printing. To tackle these challenges and be able to 3-D print the airtight vacuum bending module out of the softest TPU filament in the market (Recreus Filaflex 60 A), a regular consumer desktop FFF printer (Prusa MK3S) was modified.

To solve the filament extrusion issues, the original hotend Polytetrafluoroethylene (Teflon) tube was replaced by a Teflon tube with an inner diameter of 2.0 mm and an outer diameter of 4.0 mm. As shown in Fig. 5(a), the new Teflon is longer and the end near the nozzle was trimmed to a cone shape, the other end was trimmed to a wedge shape. Therefore, the gap between the nozzle and the Teflon tube is eliminated, and the gap between the Teflon tube and the idlers is minimized. As such, TPU filament cannot be extruded through gaps around the idler, and melted TPU will not accumulate near the nozzle. First-layer calibration was used to adjust the idler tension to an optimal extrusion of TPU filament. The first printed layer in Fig. 5(b) is expected to have no gap or visible overflow between lines, which will support a porous-less solid infill. Clogging and oozing are common issues for flexible filaments. A critical parameter that influences both the occurrence and resolution of this issue is retraction. Excessive retraction can easily cause clogging over

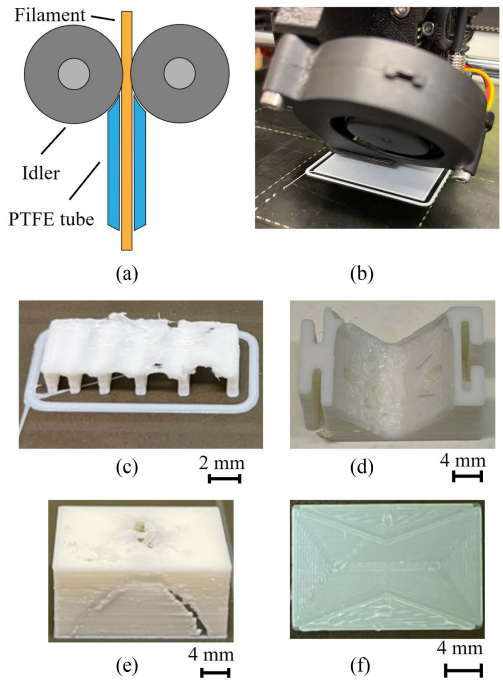

Fig. 5. 3-D printer modification and calibration. (a) The Teflon tube was replaced and cut to fit the gap between the extruder idlers. (b) First layer calibration ensures correct line width and spacing. (c) Overhang printing tests. (d) A view of the 3-D printed overhang area in a bending module, which is almost smooth with minor oozing. (e) A failed printing for a crease-based design. (f) The printing quality of a sheet with creases.

TABLE I
TPU 3-D PRINTING PARAMETERS

Parameter	Value	Unit
Resolution		
Layer height	0.1	mm
First layer height	0.2	mm
Extrusion width	0.4	mm
Retraction		
Retraction length	2	mm
Retraction speed	25	mm
Speed		
Perimeter	15	mm
Small perimeter	10	mm
External perimeter	8	mm
Bridges	8	mm
Temperature		
Nozzle	15	mm
Bed	10	mm
Fan settings		
Fan speed	70	%
Bridge fan speed	100	%
Other settings		
Infill percentage	100	%
Bridge flow ratio	1.3	1
Layer height limits	0.08-0.22	mm
Extrusion multiplier	1.2	1
Avoid crossing perimeters	Enabled	
Detect bridging perimeters	Enabled	
Fill gaps	Enabled	

time, leading to inconsistent flow rates. Conversely, insufficient retraction can result in excessive oozing and stringing, which degrade print quality, obscure details, and potentially compromise airtightness. Thus, the retraction is tuned to a moderate value through multiple printing tests (see Table I).

The module is printed with its top face on the print bed (upside down) for two reasons. First, this allows the thinnest top face to be printed directly in contact with the print bed. Second, it reduces the need for printing overhangs. However, printing overhangs is unavoidable to achieve a sufficiently long l_5 in Fig. 3(b). If l_5 is too short, it limits bending because there is not enough internal space for folding the top face and side faces. To 3-D print this overhang, a very low print speed is selected, together with a high fan speed (details in Table I), to achieve the maximum possible overhang distance. Fig. 5(c) illustrates the overhang printing quality for distances ranging from 1 to 5 mm. Based on this, the overhang distance is set to 3 mm. Fig. 5(d) illustrates the internal surface of the vacuum bending module, clearly showing that the overhang can be printed, although its surface finish is not as smooth as that of the other faces. Additional settings, as detailed in Table I, were adjusted or enabled to ensure optimal airtightness and detail. Finally, it is crucial to note that the filament was stored in an environment with relative humidity maintained below 20%. This precaution is essential because TPU filament is sensitive to moisture, which can cause bubbling during printing, resulting in poor print quality and potential clogging issues. With all printing parameter optimization, the final printed bending actuator has a good surface quality and high bending angle which can be compared to human fingers as shown in Fig. 4(d).

To demonstrate how the crease-free design enables FDM 3-D printing, a bending module with creases along the folding area (see Fig. 5 E) and a sheet with creases \(see Fig. 5 F) were fabricated using 3-D printing. Since creating creases by folding elastomers is challenging, carvings were introduced to function as creases. However, this approach results in nonuniform sheet thickness, increases the complexity of the nozzle trajectory, and requires more frequent filament extrusion and retraction. Consequently, it leads to poor printing quality, as shown in Fig. 5(e). Even when printing a flat sheet, as in Fig. 5(f), the carved trajectory causes surface irregularities and unevenness. Therefore, for 3-D printing origami-based soft actuators, the crease-free design is a critical method. It reduces the complexity of the printing trajectory and improves overall print quality, aligning with the findings of [44].

III. EXPERIMENTS AND RESULTS

A. Characterization of the Bending Module and Actuator

Based on this vacuum bending module, a vacuum bending actuator was manufactured by designing 4 modules in series and printing the entire actuator in one print using the FFF technique described earlier. Using a test bench equipped with force sensing and deformation tracking capabilities, the actuator bending angle, bending force, and hysteresis were analyzed. First, the bending angle is measured in free bending by fixing the actuator horizontally with its bending direction oriented against gravity. The bending angle is calculated by tracking a red dot on the actuator tip. The video-capturing device is the DJI

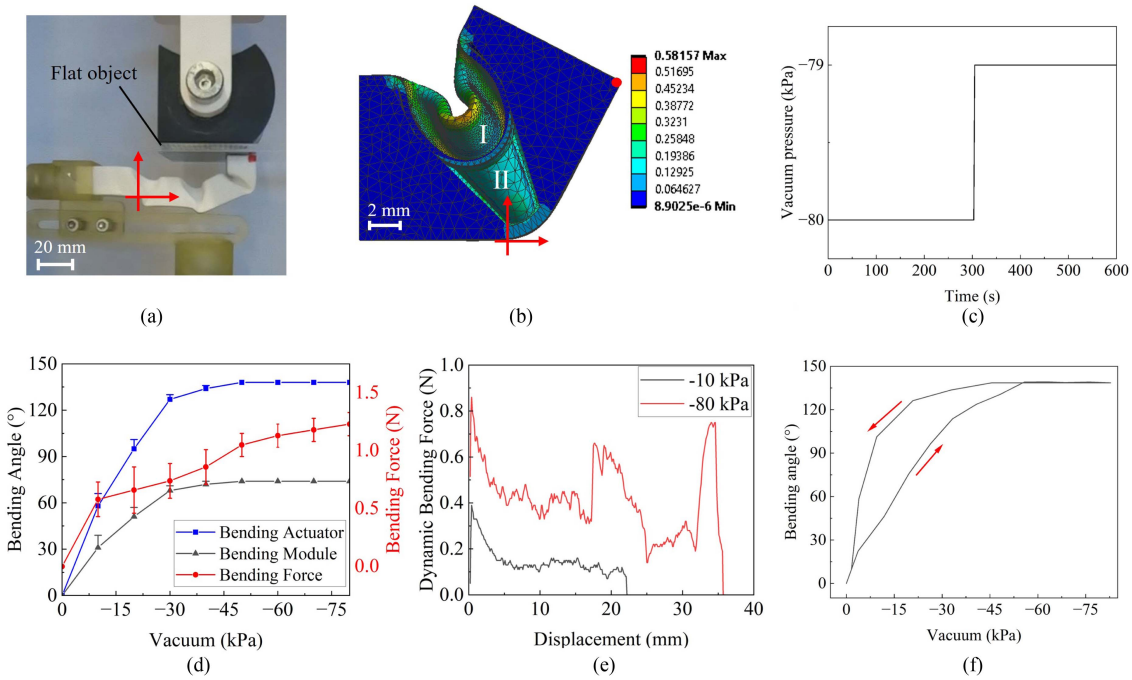

Fig. 6. Characterization of the bending module and the bending actuator. (a) The bending actuator presses against a flat surface at −80 kPa. (b) Volumetric strain contour of a bending module. (c) Vacuum pressure changes when the actuator was cut off vacuum source to test airtightness. (d) The bending angle and force of a bending actuator at different vacuum, and the bending angle of a bending module at different vacuum. (e) Bending force changes at different bending angles under actuation, the force fluctuation indicates friction occurs between the shells and the cavity interior faces. (f) Hysteresis curve of the bending actuator.

Osmo Action 3, while the vacuum sensor and regulator are the FESTO SPAN-B2R-Q4-PN-PN-L1 and the SMC IRV10-C06, respectively. The vacuum pressures are relative values regarding atmospheric pressure, and the vacuum generator is an oil-free pump, Varan Motors TC-99. The blue curve in Fig. 6(d), which shows the bending angle as a function of pressure, demonstrates the high sensitivity to pressure. It achieves its maximum bending angle of 138° at approximately −50 kPa, with each module having an individual bending angle of 74°.

The bending force is measured by clamping the bending actuator horizontally on a tensile testing machine (Tinius Olsen UTMS Model 5ST). The force exerted by the tip on the object is recorded as the bending force. The red curve in Fig. 6(d) indicates that the bending force remains at a low level, smaller than 1 N. It reaches around 0.7 N at −10 kPa, increasing with a higher vacuum. The force increment from vacuum −40 to −50 kPa is higher than the others in the range from −10 to −80 kPa. In Fig. 6(a), the bending actuator presses the object at −80 kPa. It clearly shows a distortion deformation in the middle of each module. While the high flexibility of the TPU material ensures high sensitivity to vacuum, it also leads to this low resistance to external impact, thereby limiting the maximum bending force. This shape distortion results in a slower increase in bending force after −50 kPa. The low bending force of vacuum bending actuators is primarily constrained by two factors: the limited actuation pressure (a maximum of one atmosphere) and low structural stiffness. To achieve high flexibility (more adaptive to objects), characterized by a large bending angle, the structural stiffness must remain low, even when soft materials are used, due to the inherent limitation of the actuation pressure. This article argues that the design of vacuum bending actuators should prioritize their key advantages—high adaptability and flexibility—rather than focusing on force generation. Force generation can instead be addressed through more efficient, compatible vacuum-based mechanisms, such as vacuum jamming for variable stiffness or vacuum suction cups, etc. The latter has been integrated into the octopus gripper demonstrator presented in this study, highlighting a practical and synergistic approach to enhancing overall performance.

It is worth mentioning that the deformation of the top and side faces [see Fig. 3(a)] also leads to friction between these surfaces, affecting the bending behavior at higher bending angles. This is confirmed through structural mechanics analysis in FEM on a module level of the bending actuator, as illustrated in Fig. 6(b). The simulation outcomes clearly indicate contact between the top and side faces in the cavity. This frictional contact forms even at a low vacuum of −20 kPa. To evaluate the feasibility of reducing distortion in the bending actuator in Fig. 6(a), simulations considering sheet thickness and bottom overhang length were conducted. Detailed results of these simulations are provided in Supplementary Material 1. The findings reveal that the design of vacuum bending actuators is a balance between stiffness and flexibility. Due to the inherent limitation of vacuum actuation pressure, higher structural stiffness leads to a reduction in the maximum achievable bending angle. To reach the highest flexibility, a low-stiffness design is adopted.

To further evaluate the influence of internal friction on an experimental level, a bending force test was conducted. The bending actuator was first actuated while constraining the bending tip. The constraint was then released at a speed of 0.4 mm/s, and

TABLE II
COMPARISONS WITH BENDING ACTUATORS

Actuation	Actuators	Fabrication	Materials	Bending force/ weight (N/g)	Bending angle/ length (°/mm)
Vacuum	VBA [24]	Hand made	Silicone, PE film	2/72=0.028	67/132=0.5
Vacuum	Wall-climbing [44]	Hand made	PVC and TPU	/2.57	178/52=3.4
Vacuum	V-SPA [23]	Hand made	Foam and glue	/	27.3/45=0.6
Vacuum	Vacuum-actuated [25]	Molding	Silicone (85 A)	0.42/	15/93=0.2
Vacuum	SOVAs [47]	3D printing	TPU (85 A)	3.4/13.1=0.26	80/22=3.6
Vacuum	LSOVA [53]	3D printing	TPU (85 A)	linear	linear
Vacuum	**This work**	3D printing	TPU (60 A)	0.9/2.5=0.36	74/23=3.2
Cable	VEL actuator [54]	3D printing	TPU (70 A)	4.6/	90/216=0.4
Overpressure	Multimaterial actuator [55]	molding	Diels-Alder reaction	/112	100/101=1
Bistable steel	PBRA [56]	molding	TPU, prestressed steel	3/	230/165=1.4
SMA	PBRA [57]	molding	Silicone, SMA	118.8/13.5=8.8	75/60=1.3

the bending force against the constraint object was monitored. The contact force at vacuum levels of −10 and −80 kPa is shown in Fig. 6(e). At −10 kPa, the contact force gradually decreases as the object moves away from the actuator tip, because the bending angle is small at lower vacuum levels and without significant folding behavior. At −80 kPa, although the bending force trend also decreases as the object moves away, there is significant fluctuation during the process. This fluctuation is caused by friction between the top and side faces, as well as between the object surface and the actuator tip. When the bending actuator is actuated while constrained, the top face deforms and makes contact with each other and interior faces, generating friction. This friction slightly hinders the bending. Once the bending force overcomes the static friction, the actuator bends suddenly, creating an impact that results in force peaks around displacements of 20 and 34 mm. Ultimately, the bending actuator intermittently reaches the maximum bending angle.

The hysteresis in the bending-pressure relationship of the bending actuator, occurring between actuation and deactivation, is crucial for soft robots, as it influences the actuation speed, energy efficiency, and controllability of the actuator. To investigate it, the actuator was depressurized to −80 kPa and repressurized to 0 kPa with a pressure ramp of 10 kPa per second, while the bending angle was tracked in free bending (e.g., no contact). The results in Fig. 6(f) show that the bending angle increases almost linearly during loading. However, during unloading, the angle only decreases rapidly at vacuum levels lower than –20 kPa. The hysteresis observed during the unloading phase can be attributed to two phenomena. First, it arises from internal friction between the faces of the module. However, more significantly, it is caused by buckling of the faces during actuation which leads to folding. Despite its soft and flexible nature, the bending module initially exhibits higher stiffness during bending. The actuator stiffness is reduced whenever its faces undergo buckling under loading. This instability phenomenon does not occur during unloading, in which the folds are already formed, contributing further to the hysteresis. This is a clear disadvantage of the crease-free design. In traditional origami-based soft robotic actuators, the folds/creases are inherent to the design. Hence, these actuators do not suffer from this buckling phenomenon and have superior hysteresis.

Airtightness is crucial for the energy efficiency of pneumatic actuators. To evaluate the airtightness, the actuator was vacuumed to −80 kPa and then disconnected from the vacuum source to monitor the pressure change. The blue curve in Fig. 6(c) indicates good airtightness, with the vacuum dropping only from −80 to −79 kPa after 10 min, which is a negligible loss of just 1 kPa.

To evaluate the performance of this new origami-based bending actuator, its key performance indicators, including bending force and angle are benchmarked against recently published works that present bending actuators (see Table II). The majority of comparisons focus on vacuum bending actuators since the same actuation method. To make comparison possible the bending force and angle were normalized into a force-to-weight and a bending angle-to-length ratio. The origami-based actuator, presented in this article, demonstrates the highest force-to-weight ratio and a top-tier bending-angle-to-length ratio. Only the SOVAs [47] demonstrate a higher bending-angle-to-length ratio. However, their bending mechanism differs fundamentally, relying on the tension generated by a relatively hard yet compliant thin film across the bending modules. Moreover, while the SOVAs design is compatible with FFF using stiffer materials (e.g., Shore A 85), it is not suitable for printing with softer materials such as Shore A 60, which are essential for achieving greater flexibility and compliance in soft robotic applications. Compared to other bending actuator mechanisms, such as cable-driven systems, overpressure actuation, bistable mechanisms, and stimulus– responsive materials like shape memory alloys (SMAs), vacuum bending actuators typically produce lower force. Unlike these mechanisms, the force generated by vacuum bending is inherently constrained by the limited pressure differential of one atmosphere, making significant force enhancement impractical. As a result, vacuum bending actuators should prioritize flexibility over force generation, leveraging their adaptability and compliance. For applications requiring higher bending forces, complementary methods such as vacuum granular jamming or integrated suction cups can be used to augment performance. However, for applications with stringent demands for high bending force, vacuum bending actuation may not be the optimal choice.

B. *Miniaturized Self-Closing Suction Cups*

The advantages of this new bending actuator are highlighted by the design, fabrication, and characterization of an

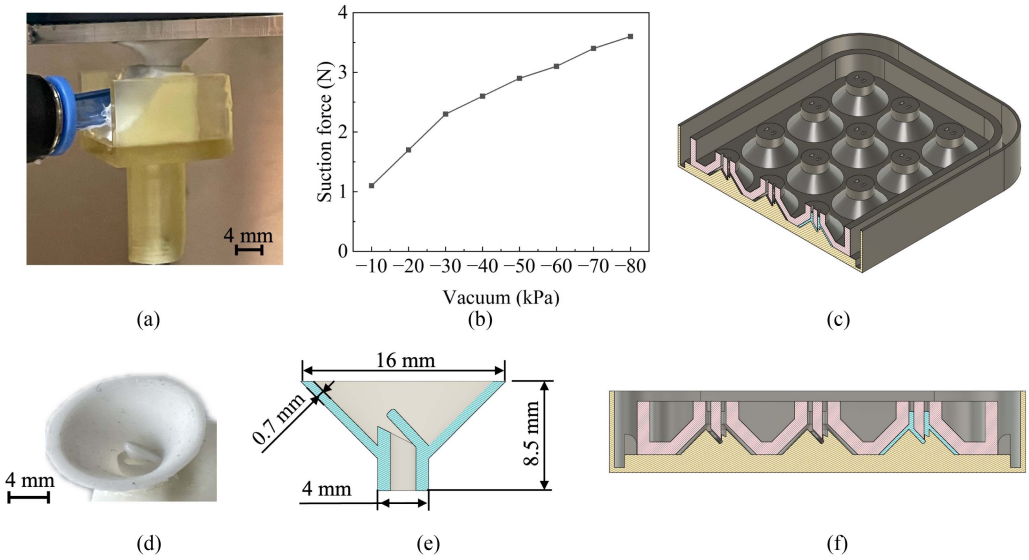

Fig. 7. Fabrication and characterization of the minimized self-closing suction cup. (a) The setup for measuring the suction force. (b) Suction force of the minimized self-closing suction cup. (c) An assembled suction cup mold. (d) The fabricated suction cup. (e) Sectional view of the suction cup. (f) Sectional view of the suction cup mold.

octopus-like redundant gripper (see Section III-C). The vacuum actuation of the bending actuator enables synchronized operation with vacuum suction cups without requiring additional systems. Conversely, the integration of vacuum suction cups enhances the overall gripping force of the vacuum bending actuators, effectively addressing their inherent limitation of low bending force. Multiple suction cups can also improve the redundancy of the gripper, as they can still generate adhesion force even when the bending actuator does not provide sufficient friction or when some suction cups are not in contact with the object. Previously published works [2], [26], [58] typically present octopus-inspired grippers composed of bending actuators either without suction cups or with suction cups actuated independently. However, integrating bending and suction within a single vacuum system poses challenges, as not all suction cups maintain contact with the object during grasping due to variations in size and shape. This can result in some suction cups remaining open, causing air leaks that reduce energy efficiency, or in loss of suction on cups that are in contact, ultimately leading to grasp failures.

In related work, self-closing suction cups can automatically self-close whenever the suction cups are not in contact with objects, thereby preventing any leaks [20]. Although compact, the design from that research was still too large for the intended vacuum bending actuator. Hence, following the same principle, this paper introduces a new design of these self-closing suction cups, scaled down to be compatible with the crease-free vacuum bending actuator. Fig. 7(e) and (d) illustrates the 3-D geometric model and molded cup, respectively. Due to the requirement for numerous suction cups and the tight tolerances of the self closing mechanism, a mold capable of producing multiple cups was 3-D printed using an SLA 3-D printer (Prusa SL1S). Fig. 7(f) provides a sectional view of the 3-D model of the mold, with the blue section line indicating the suction cup body area. The suction cup achieves its self-closing function by utilizing a soft cap that seals the vacuum port. As illustrated in Fig. 7(e), the suction cup contains a vacuum port and a cap with a thin gap. When the suction cup is not in use, the vacuum causes air to flow across the thin gap, creating an air pressure gradient around the cap. This pressure gradient forces the cap to deform, thereby sealing the vacuum port. Silicone Smooth-On Mold Max 14 NV was chosen for its exceptional flexibility (modulus of 0.24 MPa and strain at fracture of 600%), ensuring the cups can conform effectively to irregular objects and surfaces. Moreover, its low viscosity in its uncured state (7.5 Pa.s) facilitates the molding process by flowing easily into narrow gaps and corners. Fig. 7(c) displays the assembled mold, where the top mold was pressed onto the bottom mold following the casting of silicone into it. Subsequently, the mold underwent degassing in a vacuum tank.

The miniaturized self closing suction cup underwent characterization by securing it on a tensile machine (Tinius Olsen UTMS Model 5ST), depicted in Fig. 7(a). Fig. 7(b) illustrates the suction force plotted against negative pressure. This suction force notably exceeds the bending force of the crease-free vacuum bending actuator [see Fig. 5(d)]. Furthermore, measurements conducted using a pressure sensor (FESTO SPAN-B2R-Q4-PN-PN-L1) confirm that the suction cup achieves complete closure at a source vacuum pressure of -50 kPa or lower. Whenever fully closed, the suction cup will not adhere to an object anymore, even when pressed against a flat surface. At vacuum range from -20 to -40 kPa, the suction cup can still gradually adhere to a flat object when pressed against it, indicating minor leakages. However, this vacuum leakage is negligible to activate bending actuators as it does not cause a noticeable loss of vacuum.

C. Octopus-Inspired Gripper

To demonstrate the flexibility of grasping various objects, achieved through the synergy of self closing suction cups

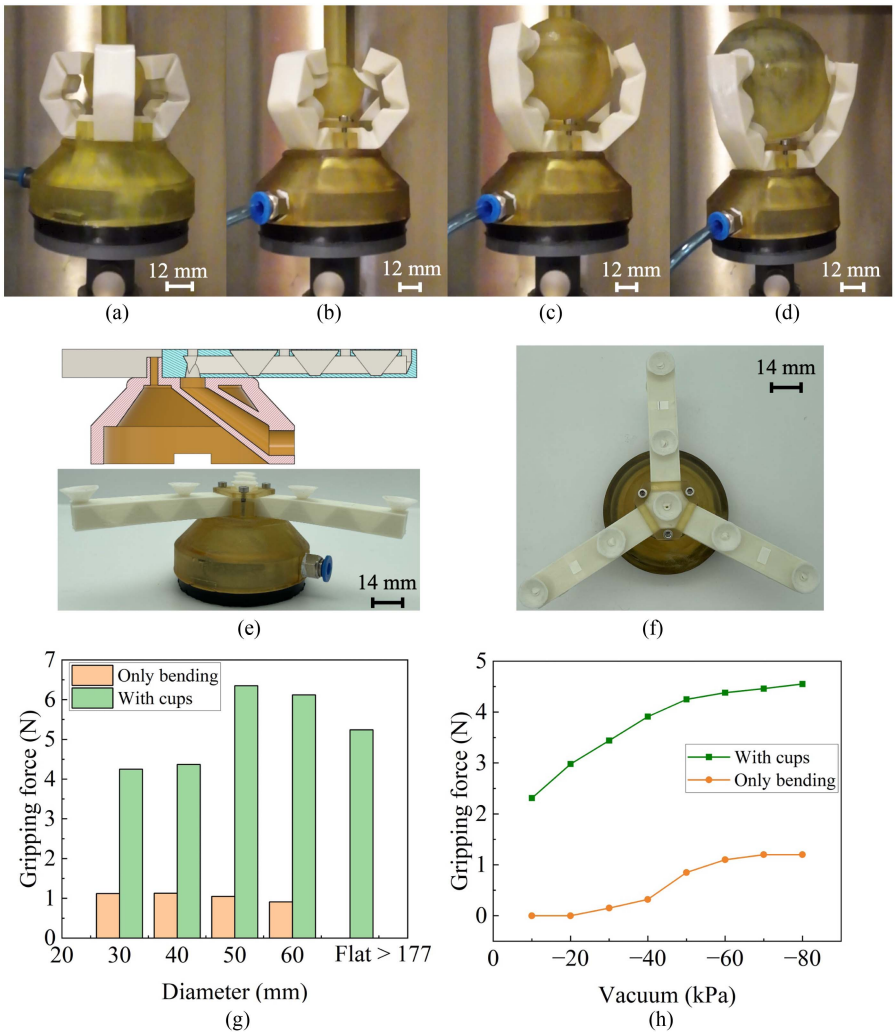

Fig. 8. Characterization of octopus-like gripper. (a) An octopus-like gripper without mini self-closing suction cups grasps a solid ball with a diameter of 40 mm. (b) An octopus-like gripper with suction cups grasps a solid ball with a diameter of 30 mm. (c) An octopus-like gripper grasps a solid ball with a diameter of 50 mm. (d) An octopus-like gripper grasps a ball with a diameter of 50 mm. (e) A sectional view and a fabricated octopus-like gripper. (f) Top view of the octopus-like gripper. (g) Influence of mini self-closing suction cups on gripping force at −80 kPa. (h) The gripping force of the octopus-like gripper on a ball with a diameter of 30 mm.

and crease-free vacuum bending actuators, we designed a new vacuum gripper. This gripper, which integrates three vacuum bending actuators, was monolithically 3-D printed. Fig. 8(e) shows the side view and sectional view of the 3-D model of the gripper. The base of the gripper is 3-D printed via SLA. Fig. 8(f) shows the top view of the fabricated octopus-like gripper. Self closing suction cups were adhered to the apertures of the bending actuators using LOCTITE 495 adhesive.

To assess the influence of suction cups in the octopus-like gripper, a comparative gripper was fabricated without suction cups for benchmarking purposes. Spherical objects were chosen as test targets because bending actuators are well-adapted to curved surfaces. Fig. 8(a) shows the vacuum gripper without suction cups grasping a sphere with a diameter of 30 mm by pressing on it, with the primary gripping force generated by friction between the actuator and the objective surface. Fig. 8(b) shows an octopus-like gripper grasping the same small object using central section cup adhesion and bending actuator friction. Although six suction cups were not in use, the total bending angle was not affected, clearly illustrating the benefit of their self closing functionality. Fig. 8(c) and (d) shows the octopus-like gripper grasping larger objects with diameters of 50 and 60 mm, respectively. The gripping force, e.g., the maximum force pulling force on the object that leads to a failure of the grasp is shown in Fig. 8(g). It is clear that the gripper that is equipped with suction cups can withstand much higher forces and this for every size of the sphere. For small spherical objects (30–40 mm) only the central suction cup is connected. Nevertheless, its gripping force is four times greater than that of a gripper without suction cups. Without suction cups, the grasp relies solely on friction, and although the use of soft materials increases adaptability and contact area, the gripper still cannot fully conform to the object. In addition, its maximum bending force is relatively small, which translates in a small gripping force. For larger objects (50–60 mm), more suction cups make contact, enhancing the gripping force. This increased contact

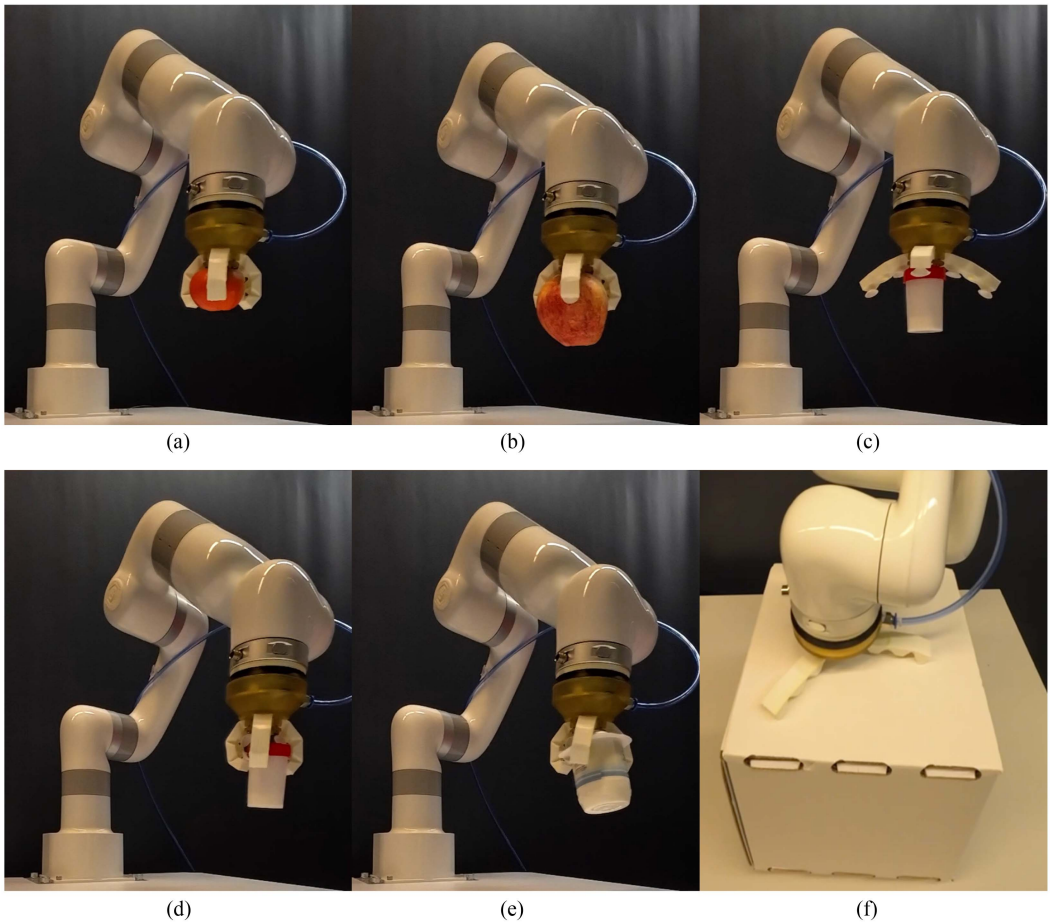

Fig. 9. Octopus-like gripper demonstrations. (a) The octopus-like gripper grasps an orange (83 g). (b) The Octopus-like gripper grasps an apple (197 g). (c) The Octopus-like gripper sucks a bottle via a central suction cup (43 g). (d) The Octopus-like gripper grips a bottle without a suction cup in use. (e) The Octopus-like gripper grasps a cup of yogurt (125 g). (f) The Octopus-like gripper lifts up a big box (170 g).

is facilitated by the high bending angle achievable with the crease-free vacuum bending actuator.

Fig. 8(h) presents the gripping force vs pressure relation of the octopus-like gripper and its benchmark gripper for grasping a small sphere with a diameter of 30 mm. Even at low vacuum of −10 kPa, the gripping with suction cups can handle higher gripping forces than the gripper without suction cups at −80 kPa, clearly demonstrating the advantages of using self closing suction cups. However, the gripping force does not significantly increase at vacuums above −50 kPa [see Fig. 8(h)]. This gripping force plateau arises because upon increasing the vacuum, the suction area of the cup decreases, which decreases its suction force. This limitation arises because the soft suction cup is tightly pressed against the surface by air pressure, which restricts the vacuum cavity area. In addition, the thin body of the suction cup stretches and slides when pulled, and any gap formation results in detachment from the surface.

In addition, a significant advantage of the octopus-like gripper is its ability to lift objects larger than the gripper itself, as long as the suction cups conform to the surface. For example, as shown in Fig. 8(g), on a flat object larger than 177 mm, which is the overall size of the gripper, the gripper can exert force greater than 5 N. This benefit arises from the fact that the suction force of the cups [see Fig. 7(b)] is larger than the bending force of the actuator [see Fig. 6(d)]. If the bending force was higher, the suction cups would detach from the object's surface, illustrating the importance of matching the suction and actuator characteristics.

The octopus-like gripper was mounted on a robot arm to demonstrate the adaptability and versatility, with a constant vacuum input of −80 kPa. Fig. 9(a) demonstrates stable grasping of an orange with a rough peel, with nearly all suction cups firmly attached to the surface. This highlights how the softness of the suction cups enables effective conformity to rough surfaces. In Fig. 9(b), an apple with an irregular shape is grasped, where a few suction cups do not make contact with the surface. Nevertheless, adequate force is generated, thanks to the flexibility of the bending actuator and the vacuum efficiency of the self closing suction cups. Furthermore, a unique example is holding a bigger object, such as a large box in Fig. 9(f). Because the bending force is substantially lower than the suction cup force, all the suction cups are tightly adhesive to the target surface rather than being peeling off by bending actuators.

The gripper can operate in various modes, including suction cup-only, contact-triggered, and bending-only modes. Fig. 9(c) demonstrates that at a low vacuum level of −20 kPa or lower, the gripper can grasp small objects without activating the bending

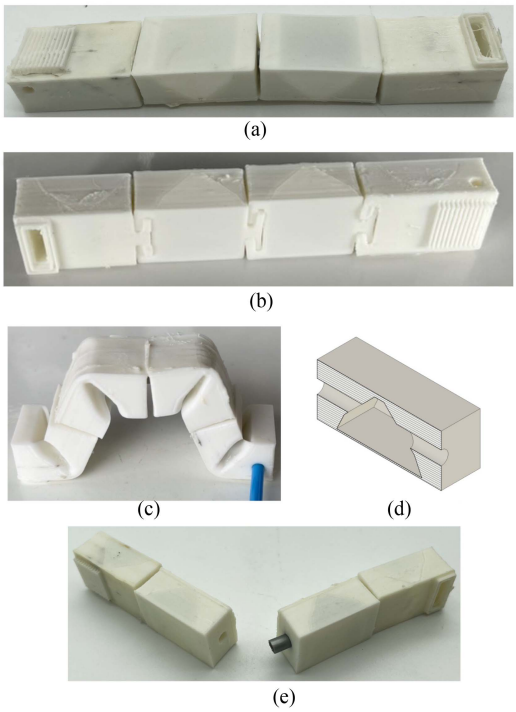

Fig. 10. Vacuum bending modules and configured locomotion robots. (a) A locomotion robot is assembled by inserting air hoses into the bending modules. (b) A locomotion robot assembled by buckling the bending modules. (c) A deformation of a locomotion robot that tightly sucks on the ground. (d) A sectional view of a bending module that can be assembled by inserting air hoses with a diameter of 4 mm. (e) A locomotion robot was being assembled via a PTGE tube (diameter 4 mm).

actuators. In this suction cup-only mode, the gripper effectively grasps multiple small lightweight targets without compressing them together. The smallest object that can be grasped must has a flat face with a bigger diameter of 16 mm to seal the suction cup. If no suction cup is mounted, because the tip of bending actuators is flat, the smallest object that can be grasped must have a diameter higher than 20 mm. This can be easily improved by modifying the actuator tip design. When the vacuum is increased to −30 kPa, as shown in Fig. 9(d), the actuators bend, resulting in additional contact between the suction cups and the objects. In this contact-triggered mode, the suction cups act as triggers for the bending action. Fig. 9(e) illustrates the bending-only mode, where a cup of yogurt is gripped by the bending actuators at −80 kPa without using the suction cups. This demonstrates that the gripper can still function even when the suction cups are not sealed, as they self-close to conserve vacuum.

D. Reconfigurable Modules and Locomotion Robots

Due to the compactness of the bending module, it can be used to create modular and reconfigurable soft actuators, Fig. 10(a). In addition, aside from actuation, the vacuum can be exploited to cohere the modules. Consequently, simple geometrical fits, including mechanical interlocking or a tube connection, respectively, in Fig. 10(b) and (e), are sufficient for creating airtight and high-strength interfaces. Fig. 10(d) shows a sectional view of the vacuum bending module, where the inner channels with a diameter of 3 mm can accommodate an air hose for its connection to other modules.

Based on this modular approach, a series of vacuum modules were used to construct two types of locomotion robots that can be reconfigured between these forms (see Fig. 11). Each robot consists of four bending modules: one with a suction cup at its end, two regular bending modules, and one with a rough surface at the end. The two robots differ in the orientation of the last module with the rough surface, which can be flipped to switch configurations. In the first configuration [see Fig. 11(a)], this last module bends inward, while in the second [see Fig. 11(b)], it bends upward. Their locomotion mechanism relies on oscillatory movement induced by a constant vacuum. Experimental results will demonstrate how this reconfiguration alters their locomotion gait.

Their oscillatory locomotion on a flat, smooth surface when connected to a constant vacuum source (-60 kPa) results from the following sequence of events: 1) Initially, airflow causes the suction cup to adhere to the surface (see Fig. 11). 2) This adhesion generates vacuum pressure that activates the bending modules, causing the soft robot to bend. 3) The bending produces a pulling force on the suction cup that eventually overcomes the suction force, causing the cup to detach. This detachment leads to a sudden loss of vacuum pressure, triggering an elastic rebound of the robot back to its original straight posture, which results in a jump. The jump is propelled forward due to increased friction at the rear end, which remains in contact with the surface. Upon landing, the cycle repeats. Thus, the robot maintains continuous forward movement as long as it is powered by vacuum and the suction cup can form a seal on the floor. The gait, or jumping frequency and distance, is altered by the reconfiguration. Whereas the first design [see Fig. 11(a)] generates a locomotion with a speed of 403 mm/s with a jumping frequency of around 3.7 Hz and a jumping distance of 109 mm, the second design [see Fig. 11(b)] generates moves with a speed of 167 mm/s, a frequency of around 3 Hz and a jumping distance of 55 mm. The reduced speed of the second configuration is attributed to the direction of the elastic force at the rear bending end, which is not oriented against the floor. Consequently, it generates less frictional force, despite the rougher surface texture of the bottom.

It is important to mention that the locomotion of these robots is also dependent on the vacuum. At −80 kPa and lower pressures, the vacuum generated by the suction cup surpasses the maximum bending force of the robot. As a result, the robot is pressed tightly to the ground and remains firmly attached, as shown in Fig. 10(c). This is because in this case, the vacuum suction force, calculated as 18 N by multiplying the vacuum pressure by the suction cup area of 36 mm^2, is significantly higher than the bending force of the actuator. For lower vacuum between −10 and −60 kPa the suction generated by the suction cup is too low to support the bending of the actuator and it detaches prior to generating the jumping movement. This highlights the importance of balancing the suction and bending force in the soft robot. Nevertheless, the locomotion can be adapted by changing the configuration of the soft robot, including changing, adding or removing bending modulus or by changing the dimensions of the suction cup or its material.

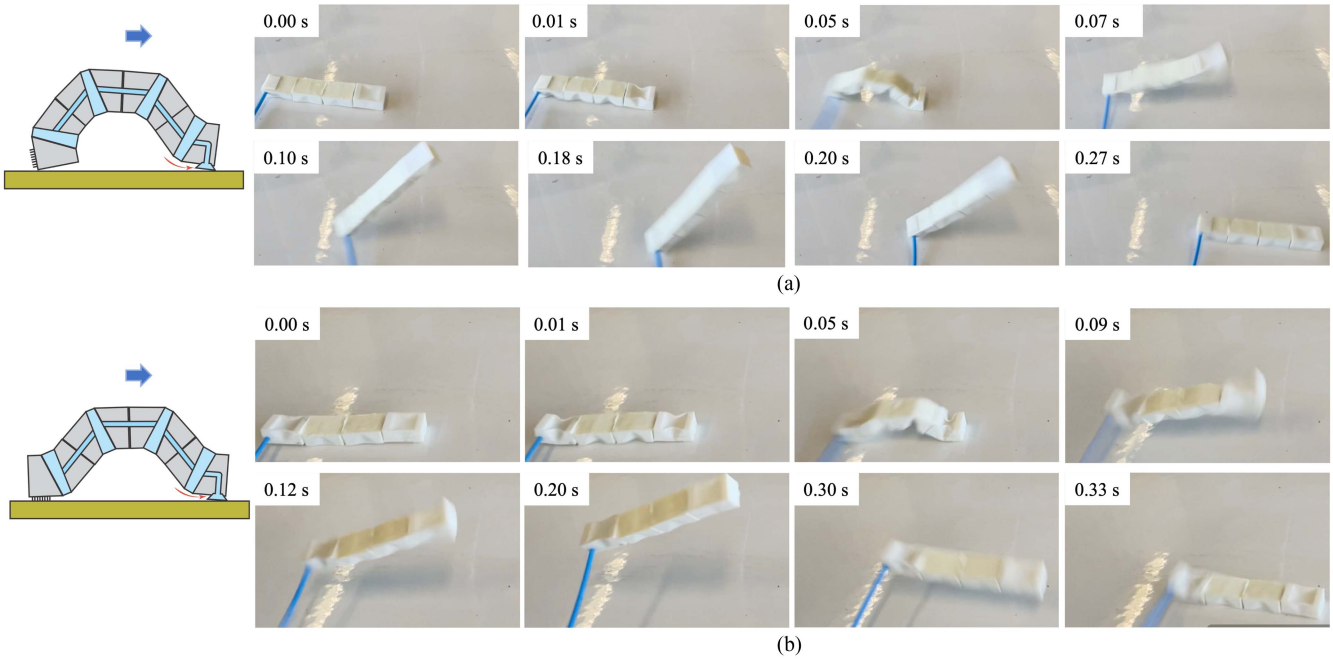

Fig. 11. Reconfigurable locomotion robots based on vacuum bending modules. (a) The locomotion robot composed of 1 suction bending end, 1 bending end, and 2 bending modules. The suction end bends upward while other modules bend downward. It was placed on a flat smooth face and connected to a vacuum pump via a flexible air hose. The robot can jump forward approximately a body length (109 mm) in around 0.3 s. (b) The locomotion robot composed of 1 suction bending end, 1 rough bending end, and 2 bending modules. The suction end and rough end bends upward while middle modules bend downward. The robot can jump forward approximately half a body length (55 mm) in around 0.3 s.

A wide variety of locomotion patterns can be generated by reconfiguring the current modules and by adding or replacing modules in the soft robot. In addition, when multiple connections are included in a single module, more complex soft robots and oscillating patterns can be generated as well. It is important to note that reconfigurability is not intended to replace 3-D printing but to complement it, as it allows the recycle used modules, saves material and time, and avoids the need for complex support structures that are difficult to remove after printing. For specific applications, such as grippers, 3-D printing remains the better choice to ensure robust performance.

IV. Conclusion

A significant focus of soft robotics research is addressing the tradeoff between compliance (softness) and force transmission through the development of novel materials, advanced designs, and control mechanisms. Despite their inherent safety and compactness, vacuum-actuated soft robots have been largely overlooked due to their relatively low force transmission and bending angles compared to positive pressure and tendon-driven actuators, which are limited by a maximum actuation pressure of one atmosphere. Origami robots, on the other hand, exhibit high flexibility. However, integrating origami mechanisms with vacuum actuation presents several challenges, including manufacturability, reliability, and material selection. Traditionally, origami robots are manually folded, which is both labor-intensive and time-consuming. Furthermore, the use of crease structures often renders actuation incompatible with pneumatic systems due to leakage risks. The formation of creases also restricts material choices to those with low elastic strain, such as plastics, metals, and paper. The application of more adaptive soft elastomers remains difficult due to the challenges associated with creating and maintaining creases.

Through theoretical analysis of origami principles, we examined how stiffness distribution enables orderly sequenced folding and deformation. Inspired by the design of an origami box, we propose a structure with varying local stiffness to optimize stiffness distribution, achieving a similar effect to crease-based origami folding. Instead of reducing stiffness in specific regions through creases, this approach enhances stiffness in selected areas to create the desired stiffness distribution. The crease-free design facilitates automated fabrication with elastomers, allowing the actuator to be 3-D printed using FFF techniques and flexible filaments with relatively low Shore hardness (60 A). In contrast, traditional designs require dense creases that complicate the nozzle movement paths during printing, and frequent extrusion and retraction can lead to parts prone to leakage.

Beyond enabling automated fabrication, the crease-free design offers several additional advantages compared to origami machines with premade creases. Eliminating sharp creases enhances durability by improving fatigue resistance, thereby extending the lifespan of the actuator during repeated cycles. The design is also fully compatible with vacuum actuation, allowing seamless integration with vacuum-driven mechanisms such as suction cups, which supports adaptable and robust robotic systems. Moreover, the crease-free surface retains the flexibility and compliance characteristic of soft elastic materials, resulting in superior conformability during contact compared to traditional origami designs with creases.

Compared to other bending actuator designs in the literature, the actuator demonstrates higher pressure sensitivity and can attain significant bending angles of 138° at the actuator level and 74° at the individual module level. The critical factor facilitating the self folding and bending behaviors of the actuator lies in the proper design of its stiffness distribution. While this article presents a structural design that eliminates the reliance on creases for origami robots, stiffness distribution can also be achieved through alternative methods, such as varying material thickness, using multimaterial compositions, or incorporating specific stimulus-responsive mechanisms.

The vacuum bending actuator offers excellent flexibility but is limited by low stiffness, resulting in low force generation. This article addresses this limitation by combining a novel crease-free origami-based bending actuator design with self-closing suction cups. The resulting soft gripper integrates three such actuators, each equipped with self-closing suction cups, providing exceptional versatility for grasping a wide range of objects. Mimicking the behavior of an octopus tentacle, the gripper operates solely using a single vacuum source. Due to the high suction force of the cups, the gripper has a high holding force, one that is much higher compared to friction-based methods. This approach is made possible by the self closing feature of suction cups. Whenever activated by vacuum, these miniaturized self closing suction cups generate adhesion force when in contact with an object, but automatically self close when not in contact. This principle is vital for the synergy between the cups and the bending angle. In addition, the combination of self closing suction cups with the actuator provides excellent versatility in picking up a variety of objects, ranging from small, round, and irregular items to those significantly larger than the gripper itself. Especially large flat objects, which are, by definition, impossible to grasp using friction alone.

Although it is possible to create the gripper and its parts using formative manufacturing (e.g., moulding), its design also allows it to print in a single print and with a single flexible filament (Shore hardness 60 A) on an FFF 3-D printer. This required modifications to the FFF 3-D printing setup, which can inspire and facilitate more potential designs and fabrications for soft robots, while also providing insights for material advancements in 3-D printing. For users of FFF printers with soft filaments, managing friction between the extruder and filaments is pivotal in ensuring sufficient and stable flow rates at the nozzle. The emergence of softer elastic 3-D printing materials holds promise for addressing challenges in soft robot development.

Finally, the research emphasizes that the crease-free vacuum bending actuator module can serve as a fundamental unit for numerous potential applications, including grippers and locomotion robots. This modular design offers opportunities for recycling actuators and streamlining 3-D printing fabrication processes, thereby mitigating issues associated with support removal. Leveraging the vacuum bending module, more intricate soft robots can be effectively fabricated.

Despite the multiple advantages offered by the novel vacuum bending actuator and its combination with self closing suction cups, several limitations persist. Currently, the 3-D printing layout of the vacuum is constrained by the need to place the thinnest layer on the printing bed for stable printing. However, this challenge can potentially be addressed through multimaterial 3-D printing, which can generate supports with different materials for the TPU thin layer. Moreover, while the force transmission of vacuum systems can be enhanced by integrating suction cups, typically sufficient for standard applications, the ultimate adhesion power remains constrained by atmospheric conditions. This limitation may impede the applicability of the actuator for heavier tasks. However, variable stiffness techniques such as granular jamming or other related vacuum technologies are complementary approaches that can significantly enhance the maximum payload capacity of vacuum actuators. Future research will explore sequential vacuum actuation strategies, involving bending, suction, and subsequent granular jamming, within the entire vacuum end-effector system.

REFERENCES

[1] R. Chen, X. Tao, C. Cao, P. Jiang, J. Luo, and Y. Sun, "A Soft, Lightweight flipping robot with versatile motion capabilities for wall-climbing applications," *IEEE Trans. Robot.*, vol. 39, no. 5, pp. 3960–3976, Oct. 2023.

[2] Z. Xie et al., "Octopus arm-inspired tapered soft actuators with suckers for improved grasping," *Soft Robot.*, vol. 7, no. 5, pp. 639–648, Oct. 2020.

[3] X. Qi, H. Shi, T. Pinto, and X. Tan, "A novel pneumatic soft snake robot using traveling-wave locomotion in constrained environments," *IEEE Robot. Automat. Lett.*, vol. 5, no. 2, pp. 1610–1617, Apr. 2020.

[4] M. Leveziel, W. Haouas, G. J. Laurent, M. Gauthier, and R. Dahmouche, "MiGriBot: A miniature parallel robot with integrated gripping for high-throughput micromanipulation," *Sci. Robot.*, vol. 7, no. 69, Aug. 2022, Art. no. eabn4292.

[5] H. Yuk, B. Lu, and X. Zhao, "Hydrogel bioelectronics," *Chem. Soc. Rev.*, vol. 48, no. 6, pp. 1642–1667, 2019.

[6] R. S. Diteesawat, T. Helps, M. Taghavi, and J. Rossiter, "Electro-pneumatic pumps for soft robotics," *Sci. Robot.*, vol. 6, no. 51, Feb. 2021, Art. no. 3721.

[7] Y. Dong et al., "Untethered small-scale magnetic soft robot with programmable magnetization and integrated multifunctional modules," *Sci. Adv.*, vol. 8, no. 25, Jun. 2022, Art. no. eabn8932.

[8] Q. Ze et al., "Spinning-enabled wireless amphibious origami millirobot," *Nature Commun.*, vol. 13, no. 1, Dec. 2022, Art. no. 3118.

[9] X. Fan et al., "Scale-reconfigurable miniature ferrofluidic robots for negotiating sharply variable spaces," *Sci. Adv.*, vol. 8, no. 37, Sep. 2022, Art. no. eabq1677.

[10] R. Coulson, C. J. Stabile, K. T. Turner, and C. Majidi, "Versatile soft robot gripper enabled by stiffness and adhesion tuning via thermoplastic composite," *Soft Robot.*, vol. 9, no. 2, pp. 189–200, Apr. 2022.

[11] J. A.-C. Liu, J. H. Gillen, S. R. Mishra, B. A. Evans, and J. B. Tracy, "Photothermally and magnetically controlled reconfiguration of polymer composites for soft robotics," *Sci. Adv.*, vol. 5, no. 8, Aug. 2019, Art. no. eaaw2897.

[12] D. Schönfeld, D. Chalissery, F. Wenz, M. Specht, C. Eberl, and T. Pretsch, "Actuating shape memory polymer for thermoresponsive soft robotic gripper and programmable materials," *Molecules*, vol. 26, no. 3, p. 522, Jan. 2021.

[13] Z. Li, N. V. Myung, and Y. Yin, "Light-powered soft steam engines for self-adaptive oscillation and biomimetic swimming," *Sci. Robot.*, vol. 6, no. 61, Dec. 2021, Art. no. eabi4523.

[14] I. Katz, T. Shomrat, and N. Nesher, "Feel the light: Sight-independent negative phototactic response in octopus arms," *J. Exp. Biol.*, vol. 224, no. 5, Mar. 2021, Art. no. jeb237529.

[15] M. D. Soorati, M. K. Heinrich, J. Ghofrani, P. Zahadat, and H. Hamann, "Photomorphogenesis for robot self-assembly: Adaptivity, collective decision-making, and self-repair," *Bioinspiration Biomimetics*, vol. 14, no. 5, Sep. 2019, Art. no. 056006.

[16] A. Pagoli, F. Chapelle, J.-A. Corrales-Ramon, Y. Mezouar, and Y. Lapusta, "Review of soft fluidic actuators: Classification and materials modeling analysis," *Smart Mater. Structures*, vol. 31, no. 1, Jan. 2022, Art. no. 013001.

[17] S. Song, D.-M. Drotlef, D. Son, A. Koivikko, and M. Sitti, "Adaptive self-sealing suction-based soft robotic gripper," *Adv. Sci.*, vol. 8, no. 17, Sep. 2021, Art. no. 2100641.

[18] T. M. Huh et al., "A multi-chamber smart suction cup for adaptive gripping and haptic exploration," in *Proc. IEEE/RSJ Int. Conf. Intell. Robots Syst.*, Prague, Czech Republic, IEEE, Sep. 2021, pp. 1786–1793.

[19] T. Yue et al., "A contact-triggered adaptive soft suction cup," *IEEE Robot. Automat. Lett.*, vol. 7, no. 2, pp. 3600–3607, Apr. 2022.

[20] Z. Wang et al., "Self-closing and self-healing multi-material suction cups for energy-efficient vacuum grippers," *Adv. Intell. Syst.*, vol. 5, no. 10, 2023, Art. no. 2300135.

[21] H. Wang, S. Terryn, Z. Wang, G. Van Assche, F. Iida, and B. Vanderborght, "Self-regulated self-healing robotic gripper for resilient and adaptive grasping," *Adv. Intell. Syst.*, vol. 5, no. 12, 2023, Art. no. 2300223.

[22] E. Brown et al., "Universal robotic gripper based on the jamming of granular material," *Proc. Nat. Acad. Sci.*, vol. 107, no. 44, pp. 18809–18814, Nov. 2010.

[23] M. A. Robertson and J. Paik, "New soft robots really suck: Vacuum-powered systems empower diverse capabilities," *Sci. Robot.*, vol. 2, no. 9, Aug. 2017, Art. no. eaan6357.

[24] S. D. Katugampala, K. M. S. Arachchi, S. Asanka, R. B. Arumathanthri, A. L. Kulasekera, and N. D. Jayaweera, "Design and characterization of a novel vacuum bending actuator and a bimorph: For preliminary use in a continuum robot arm," in *Proc. IEEE Int. Conf. Cybern. Intell. Syst. IEEE Conf. Robot., Automat. Mechatron.*, Bangkok, Thailand, IEEE, Nov. 2019, pp. 263–268.

[25] J. Miller and N. Wicks, "Vacuum-actuated bending for grasping," *Robotics*, vol. 7, no. 4, p. 73, Nov. 2018.

[26] B. Mazzolai et al., "Octopus-inspired soft arm with suction cups for enhanced grasping tasks in confined environments," *Adv. Intell. Syst.*, vol. 1, no. 6, Oct. 2019, Art. no. 1900041.

[27] M. Wu et al., "Glowing Sucker octopus (stauroteuthis syrtensis)-inspired soft robotic gripper for underwater self-adaptive grasping and sensing," *Adv. Sci.*, vol. 11, 2022, Art. no. 2104382.

[28] J. A. Faber, A. F. Arrieta, and A. R. Studart, "Bioinspired spring origami," *Science*, vol. 359, no. 6382, pp. 1386–1391, Mar. 2018.

[29] F. Haas, S. Gorb, and R. J. Wootton, "Elastic joints in dermapteran hind wings: Materials and wing folding," *Arthropod Struct. Develop.*, vol. 29, no. 2, pp. 137–146, Apr. 2000.

[30] H. Kobayashi, B. Kresling, and J. F. V. Vincent, "The geometry of unfolding tree leaves," *Proc. Roy. Soc. B: Biol. Sci.*, vol. 265, no. 1391, pp. 147–154, Jan. 1998.

[31] Z. Zhai, Y. Wang, K. Lin, L. Wu, and H. Jiang, "In situ stiffness manipulation using elegant curved origami," *Sci. Adv.*, vol. 6, no. 47, Nov. 2020, Art. no. eabe2000.

[32] S. Li, D. M. Vogt, D. Rus, and R. J. Wood, "Fluid-driven origami-inspired artificial muscles," *Proc. Nat. Acad. Sci.*, vol. 114, no. 50, pp. 13132–13137, Dec. 2017.

[33] Z. Zhakypov, F. Heremans, A. Billard, and J. Paik, "An origami-inspired reconfigurable suction gripper for picking objects with variable shape and size," *IEEE Robot. Automat. Lett.*, vol. 3, no. 4, pp. 2894–2901, Oct. 2018.

[34] C. Geckeler and S. Mintchev, "Bistable helical origami gripper for sensor placement on branches," *Adv. Intell. Syst.*, vol. 4, no. 10, Oct. 2022, Art. no. 2200087.

[35] S. Zhang, X. Ke, Q. Jiang, H. Ding, and Z. Wu, "Programmable and reprocessable multifunctional elastomeric sheets for soft origami robots," *Sci. Robot.*, vol. 6, no. 53, Apr. 2021, Art. no. eabd6107.

[36] D. Rus and M. T. Tolley, "Design, fabrication and control of soft robots," *Nature*, vol. 521, no. 7553, pp. 467–475, Jun. 2018.

[37] S. R. Kashef, S. Amini, and A. Akbarzadeh, "Robotic hand: A review on linkage-driven finger mechanisms of prosthetic hands and evaluation of the performance criteria," *Mechanism Mach. Theory*, vol. 145, Mar. 2020, Art. no. 103677.

[38] Y. Liu, Z. Ge, S. Yang, I. D. Walker, and Z. Ju, "Elephant's trunk robot: An extremely versatile under-actuated continuum robot driven by a single motor," *J. Mechanisms Robot.*, vol. 11, no. 051008, Jul. 2019.

[39] C. Liu, P. Maiolino, and Z. You, "A 3D-Printable robotic gripper based on thick panel origami," *Front. Robot. AI*, vol. 8, Sep. 2021.

[40] C. Liu, P. Maiolino, Y. Yang, and Z. You, "Hybrid soft-rigid deployable structure inspired by thick-panel origami," in *Proc. ASME 2020 Int. Des. Eng. Tech. Conf.s Comput. Inf. Eng. Conf.*. American Society of Mechanical Engineers Digital Collection, Nov. 2020.

[41] Z. Kan, Y. Zhang, Y. Yang, Y. A. Tse, and M. Y. Wang, "An origami-inspired monolithic soft gripper based on geometric design method," in *Proc. IEEE 2nd Int. Conf. Soft Robot.*, Apr. 2019, pp. 470–476.

[42] K. Lee, Y. Wang, and C. Zheng, "TWISTER hand: Underactuated robotic gripper inspired by origami twisted tower," *IEEE Trans. Robot.*, vol. 36, no. 2, pp. 488–500, Apr. 2020.

[43] D. Li et al., "Origami-inspired soft twisting actuator," *Soft Robot.*, vol. 10, no. 2, pp. 395–409, Apr. 2023.

[44] Y. Zhai et al., "Desktop fabrication of monolithic soft robotic devices with embedded fluidic control circuits," *Sci. Robot.*, vol. 8, no. 79, Jun. 2023, Art. no. eadg3792.

[45] J. D. Hubbard et al., "Fully 3D-printed soft robots with integrated fluidic circuitry," *Sci. Adv.*, vol. 7, no. 29, Jul. 2021, Art. no. eabe5257.

[46] T. J. Wallin, J. Pikul, and R. F. Shepherd, "3D printing of soft robotic systems," *Nature Rev. Mater.*, vol. 3, no. 6, pp. 84–100, May 2018.

[47] C. Tawk, M. in het Panhuis, G. M. Spinks, and G. Alici, "Bioinspired 3D printable soft vacuum actuators for locomotion robots, grippers and artificial muscles," *Soft Robot.*, vol. 5, no. 6, pp. 685–694, Dec. 2018.

[48] A. Zatopa, S. Walker, and Y. Menguc, "Fully soft 3D-Printed electroactive fluidic valve for soft hydraulic robots," *Soft Robot.*, vol. 5, no. 3, pp. 258–271, Jun. 2018.

[49] M. Schaffner, J. A. Faber, L. Pianegonda, P. A. Rühs, F. Coulter, and A. R. Studart, "3D printing of robotic soft actuators with programmable bioinspired architectures," *Nature Commun.*, vol. 9, no. 1, p. 878, Dec. 2018.

[50] O. Bliah, S. Joe, R. Reinberg, A. B. Nardin, L. Beccai, and S. Magdassi, "3D printing stretchable and compressible porous structures by polymerizable emulsions for soft robotics," *Mater. Horiz.*, vol. 10, pp. 4976–4985, 2023.

[51] E. F. Gomez et al., "3D-Printed self-healing elastomers for modular soft robotics," *ACS Appl. Mater. Interfaces*, vol. 13, no. 24, pp. 28870–28877, Jun. 2021.

[52] K. M. Hurlbutt, "Silicone resins for vat polymerization printing," Los Alamos National Laboratory (LANL), Los Alamos, NM (United States), Tech. Rep. LA-UR-24-22087, Mar. 2024.

[53] C. Tawk, G. M. Spinks, M. in het Panhuis, and G. Alici, "3D printable vacuum-powered soft linear actuators," in *Proc. IEEE/ASME Int. Conf. Adv. Intell. Mechatron.*. Hong Kong, China, IEEE, Jul. 2019, pp. 50–55.

[54] P. Kappel, L. Kürner, T. Speck, and F. Tauber, "A pneumatic bending actuator system inspired by the avian tendon locking mechanism," in *Biomimetic Biohybrid System*, F. Meder, A. Hunt, L. Margheri, A. Mura, and B. Mazzolai, Eds, vol. 14158. Cham, Switzerland: Springer, 2023, pp. 84–100.

[55] Z. Wang et al., "Topology optimized multi-material self-healing actuator with reduced out of plane deformation," in *Proc. IEEE/RSJ Int. Conf. Intell. Robots Syst.*, Oct. 2022, pp. 5448–5455.

[56] X. Wang, A. Khara, and C. Chen, "A soft pneumatic bistable reinforced actuator bioinspired by venus flytrap with enhanced grasping capability," *Bioinspiration Biomimetics*, vol. 15, no. 5, Aug. 2020, Art. no. 056017.

[57] X. An, Y. Cui, H. Sun, Q. Shao, and H. Zhao, "Active-cooling-in-the-Loop controller design and implementation for an SMA-Driven soft robotic tentacle," *IEEE Trans. Robot.*, vol. 39, no. 3, pp. 2325–2341, Jun. 2023.

[58] B. Mazzolai, L. Margheri, M. Cianchetti, P. Dario, and C. Laschi, "Soft-robotic arm inspired by the octopus: II. from artificial requirements to innovative technological solutions," *Bioinspiration Biomimetics*, vol. 7, no. 2, Jun. 2012, Art. no. 025005.